Original Research

Quantitative T_2 in the Occipital Lobe: The Role of the CPMG Refocusing Rate

Bojana Stefanovic, BS,* John G. Sled, PhD, and G. Bruce Pike, PhD

Purpose: To investigate the dependence of occipital gray and white matter T_2 on the Carr-Purcell-Meiboom-Gill (CPMG) refocusing interval, thereby testing the basis of a novel functional magnetic resonance imaging (fMRI) method for blood volume quantification, and addressing recent questions surrounding T_2 contrast in the occipital lobe.

Materials and Methods: A CPMG sequence with $1 \times 1 \times 5$ mm^3 resolution was used to quantify T_2 in a single axial slice at the midlevel of the occipital lobe in 23 healthy adult volunteers. Refocusing intervals of 8, 11, and 22 msec were compared. A Bayesian classifier was used to classify a $1 \times 1 \times 1$ mm^3 T_1-weighted three-dimensional data set into gray matter, white matter, and cerebrospinal fluid, with an average 95% a posteriori probability used as the threshold for inclusion into a tissue-specific region of interest (ROI).

Results: The usual T_2 contrast between the gray and white matter (i.e., $T_{2GM} > T_{2WM}$) was observed, with a highly significant effect of tissue type on the estimated T_2 ($P < 10^{-5}$). The observed T_2 gradually decreased with increasing refocusing interval, for a decrease of 3.3 ± 1.5 msec in gray matter and 3.0 ± 1.5 msec in white matter between the 8 and 22 msec refocusing interval acquisitions.

Conclusion: The observed T_2 shortening is consistent with the effect of the dramatic decrease in T_2 of partly deoxygenated blood on this range of refocusing rates.

Key Words: T_2 relaxation; occipital lobe; refocusing rate; tissue T_2 contrast; blood
J. Magn. Reson. Imaging 2003;18:302–309.

THE DIFFERENCE IN the rates of transverse relaxation between various tissues represents a fundamental source of contrast in magnetic resonance imaging (MRI). Quantification of T_2 is important for optimization of acquisition parameters, longitudinal examinations, direct comparisons between studies, and enhancement of pathologic specificity. Furthermore, T_2 relaxometry has recently been used to measure hemodynamic and metabolic parameters fundamental to brain function investigations (1).

A plethora of T_2 quantification studies established slower transverse decay in the gray matter (GM) vs. white matter (WM) of healthy adult brain (2–4). This common T_2 ordering is thought to primarily reflect the rapid decay of the myelin-associated water in combination with the preponderance of myelin sheath in the WM (5). However, a significant amount of regional heterogeneity within each tissue has been documented (5,6). Moreover, dramatic age-specific variations have been reported: most notably, an inversion of the common gray-white matter T_2 contrast in the newborn, hypothesized to result from incomplete myelination (7). A shortening of T_2 has been observed in the deep GM structures of the extrapyramidal system (8–10), as well as in the cerebral cortices (11–13). While this enhanced transverse decay is very frequently postulated to arise from progressive accumulation of ferritin with age, a number of rigorous quantitative relaxometry studies showed no correlation between tissue iron concentration and T_2 across different brain regions (14–16). In particular, having quantified T_2 via both MRI and magnetic resonance spectroscopy (MRS) in a set of cadaveric brains, Chen et al (14) performed quantitative assays for iron and ferritin of the same specimens, but found no consistent correlation between either ferritin or iron concentration and T_2 values. Recently, an inversion of T_2 contrast between GM and WM in the occipital lobe of healthy adults has been reported at 1.5 T at $1 \times 1.3 \times 2$ mm^3 resolution and hypothesized to result from larger ferritin deposits in the occipital GM (vs. WM) (17). Another recent study also documented shorter T_2 in GM than in WM of the occipital lobe at both 4 T and 7 T (18).

In addition to T_2 shortening, the presence of an agent of high magnetic susceptibility, such as ferritin in oligodendrocytes (19), may give rise to a dependence of T_2 on the interval between the refocusing pulses (τ_{180}) in a Carr-Purcell-Meiboom-Gill (CPMG) experiment. Specifically, T_2 is expected to decrease with refocusing interval elongation due to increased extent to which water molecules sample the magnetically inhomogeneous en-

McConnell Brain Imaging Centre, Montreal Neurological Institute, McGill University, Montreal, Canada.

Contract grant sponsor: Natural Sciences and Engineering Research Council of Canada; Contract grant sponsor: Canadian Institutes of Health Research.

This work was presented in part at the 10th Annual Meeting of ISMRM, Honolulu, Hawaii, 2002.

*Address reprint requests to: B.S., McConnell Brain Imaging Centre, Montreal Neurological Institute, 3801 University Street, WB325, Montreal, Quebec H3A 2B4 Canada. Email: bojana@bic.mni.mcgill.ca

Received December 17, 2002; Accepted May 14, 2003.

DOI 10.1002/jmri.10360

Published online in Wiley InterScience (www.interscience.wiley.com).

vironment surrounding the agent within an interecho interval (20). This phenomenon has been extensively studied both in iron-rich GM (8,9,14,19) and in blood, where partial deoxygenation leads to the production of paramagnetic deoxyhemoglobin (dHb) (21–23). Indeed, in the context of functional MRI (fMRI), we have developed a technique for measurement of activation-induced blood volume changes that achieves blood signal isolation at 1.5 T by assuming that only the T_2 of blood (vs. those of tissues) changes with the refocusing interval (24). Contrary to this assumption, albeit at higher fields, a recent study reported very pronounced occipital gray and white matter T_2 dependencies on the refocusing rate at both 4 T and 7 T, the estimated T_2 decreasing by 30%–40% between a short (6–7 msec) and a set of long (more than 10 msec) refocusing interval acquisitions (18). While a greater decrease of the blood T_2 with refocusing interval elongation is expected at higher fields, the overall shortening of blood T_2 in combination with low tissue blood content makes it unlikely that the blood T_2 dependence on the refocusing interval alone fully explains these findings.

In view of the reported magnitude of tissue T_2 shortening with increasing refocusing interval at 4 T and 7 T suggesting an extravascular source of this dependency, we set out to explore this phenomenon at 1.5 T. We thus investigated the refocusing rate dependence of T_2 in GM and WM in the occipital lobe of a large group of healthy human volunteers at 1.5 T. We hypothesized that the variation of the refocusing intervals in the range of interest produces no effect on the extravascular brain tissue T_2. The measurements were obtained using a 32-echo CPMG sequence with three different refocusing intervals, namely 8, 11, and 22 msec. Due to the potential of voxels partially filled by cerebrospinal fluid (CSF) to confound the tissue T_2 relaxometry, we sought to define regions of interest (ROIs) with minimal partial volume contamination. At the same time, we aimed to include as many voxels in our ROIs as possible, maximizing both SNR and the robustness of our T_2 estimates. Therefore, we used a manually-trained Bayesian classifier, supplied with high resolution ($1 \times 1 \times 1$ mm^3) T_1-weighted volumes, to identify gray, white, and CSF regions having a small likelihood of contamination by other tissues. Nonlinear least squares minimization was performed to fit the echoes to a monoexponential model. We present the estimated T_2 values in each region of interest. The results of a multifactor analysis of variance of the T_2 estimates, as well as direct comparisons, are provided, illustrating the effects of tissue type and refocusing interval on T_2 values, while controlling for intersubject variability.

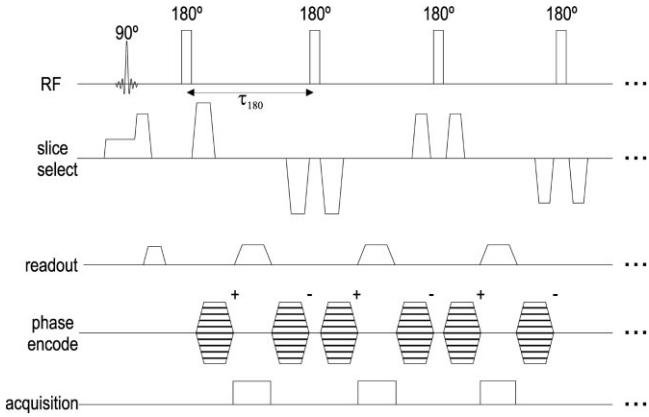

Figure 1. Schematic of the CPMG sequence used for T_2 quantification. The spoiler gradients in the slice-select direction alternate in sign and decrease in magnitude with each echo. The refocusing interval (τ_{180}) is respectively set to 8, 11, and 22 msec in the three CPMG sequence variants employed.

MATERIALS AND METHODS

Measurements

The experimental protocol consisted of a three-dimensional radiofrequency (RF)-spoiled T_1-weighted gradient echo ($1 \times 1 \times 1$ mm^3) sequence for tissue classification purposes; followed by three versions of a 32-echo single-slice CPMG ($1 \times 1 \times 5$ mm^3) sequence for T_2 quantification. The single slice for the CPMG acquisitions was located axially, at the midline of the occipital lobe and positioned to exactly span five 1-mm slices of the T_1-weighted volumetric acquisition. The head of the subject was immobilized using a vacuum bag, and all acquisitions were obtained in a single session to minimize the probability of misregistration. Twenty-three healthy adult volunteers were studied (10 women and 13 men), with an age distribution of 29 ± 5 years (mean ± SD), and a range of 24 to 42 years. In view of a very slow increase in occipital cortex iron levels after the first two decades of life (11), this age range ensured minimal differences between iron levels in the occipital cortices of the subjects. Informed consent was obtained before each session in accordance with institution guidelines. The first four subjects were examined on a Siemens 1.5-T Magnetom Vision system, and the remaining 19 on a Siemens 1.5-T Magnetom Sonata system (following upgrade). The high resolution gradient-echo sequence used a 256-mm field of view (FOV), 256×256 matrix, TR/TE of 22/10 msec, and nonselective 30° RF-spoiled excitation. The CPMG sequence is illustrated schematically in Figure 1. The interecho intervals in the three CPMG sequence versions were 8, 11, and 22 msec. This choice was driven by the range of refocusing rates employed in our cerebral blood volume (CBV) methodology, optimal sensitivity to potential ferritin-induced T_2 shortening (based on the T_2 relaxometry data from the extrapyramidal system [9]) in combination with hardware limitations, power deposition considerations, gradient performance, spatial encoding, and signal-to-noise ratio (SNR) requirements (25). The sequence parameters were optimized to provide robust T_2 measurements with the shortest achievable interecho intervals, given the primary motivation of investigating the T_2 dependence on a range of refocusing intervals of interest for our CBV methodology. The three CPMG variants were played out in randomized order. To minimize the confounding effects of imperfect slice profiles and sensitivity to B_1 inhomogeneities, nonselective composite $90°_x - 180°_y - 90°_x$ pulses were used for refocusing. To suppress stimulated echoes, flow effects,

and signal contributions outside of the slice of interest, the refocusing pulses were flanked by spoiling gradients, alternating in sign and decreasing in magnitude (26). The total diffusion weighting due to these gradients was small, with b-value less than one second/mm^2 in the last echo. Identical crusher gradient amplitudes and timing with respect to the refocusing pulses in all three versions of the CPMG sequence ensured identical b-values. A 256-mm FOV, with a 256×256 matrix, and a two second repetition time were used in each CPMG acquisition. The total scan time per subject was approximately 40 minutes.

Data Analysis

Masks of the occipital lobe were manually defined on the volumetric T_1-weighted data. Tissue segmentation within these masks was then performed using a parametric Bayesian approach that assumes the voxel intensities are drawn from a mixed population of three statistical distributions (GM, WM, and CSF) (27). Only voxel intensities from the T_1-weighted 1-mm isotropic resolution scans were considered in the segmentation process. All class conditional probability distributions were assumed to be Gaussian; and the class prior probabilities were equal for the three classes. For each subject, three sets of 100 manually selected voxels belonging to each of GM, WM, or CSF were used to compute mean intensity and SD for each class. This training data set allowed an explicit calculation of the parametric estimates of the a posteriori probabilities as scaled likelihoods of voxel intensity value given that the voxel belongs to a class, in accordance with the Bayes's theorem (28).

The Bayes classification produced three normalized a posteriori probability maps, respectively specifying the probabilities of voxels belonging to GM, WM, or CSF. From each of these probability maps, we selected the five 1-mm axial slices contained in the 5-mm transverse slice of the CPMG acquisitions. Thereafter, a careful visual inspection of multimodal overlaid data, on a subject-by-subject basis, was performed to check for intrascan movement and ensure the spatial alignment of the three-dimensional T_1-weighted scan and the CPMG data set. The threshold for inclusion of a $1 \times 1 \times 5$ mm^3 voxel from the CPMG slice into a tissue specific ROI was a 95% average of normalized a posteriori probabilities of the five corresponding $1 \times 1 \times 1$ mm^3 voxels from the three-dimensional T_1-weighted data. The resulting GM ROI, for example, was composed only of voxels having at least 95% probability of being GM, with average normalized a posteriori probability of CSF of 0.6 ± 0.4%. This analysis approach thus afforded rigorous minimization of partial volume errors while maximizing the SNR and, hence, T_2 estimation accuracy.

For each echo time, the CPMG data from all voxels within each ROI were averaged. The first two echoes of the 8-msec acquisition, the first echo of the 11-msec acquisition; as well as the last nine echoes of the 11-msec acquisition and the last 20 echoes of the 22-msec acquisition were discarded to ensure comparable temporal sampling windows (namely, 24–256 msec, 22–253 msec, and 22–264 msec for 8-, 11-, and 22-msec acquisitions, respectively). Nonlinear least squares minimization (via the Nelder-Mead Simplex method) was used for fitting of the resulting decay curves to a monoexponential decay model. Multiexponential fitting was explored, but afforded no additional information, and was hence discontinued. This result was expected, because the sampling time window, from ~20 to ~260 msec, used for fitting resulted in a much reduced myelin water contribution (5) and was insufficient for robust detection of the CSF peak (with the CSF contribution expected to be minimal, anyhow, given the stringent ROI selection procedure). Three-factor analysis of variance (ANOVA) was used to investigate the effects of tissue type, refocusing interval, and intersubject variability on the estimated transverse relaxation time constant. Tukey's procedure was employed post hoc to identify significant pairwise differences.

RESULTS

Sample ROIs produced by Bayesian classification of a subject's T_1 data, followed by averaging and thresholding at the 95% level (as described above), are shown in Figure 2a and b. The corresponding plots (Fig. 2c and d) show the logarithm of averaged ROI signal intensities from the last 30 echoes of the 8-msec echo spacing acquisition and the logarithm of the corresponding fitted values in the same subject.

The T_2 data for the 23 subjects are listed and summarized in Tables 1 and 2, for WM and GM, respectively. The average normalized Bayesian a posteriori probabilities for the WM ROIs were 99 ± 0, 1.0 ± 0.4, and 0.0 ± 0.0% for WM, GM, and CSF, respectively. For the GM ROIs, the average a posteriori probabilities were 99 ± 1, 0.7 ± 0.4, and 0.6 ± 0.4% for GM, WM, and CSF, respectively. The errors in T_2 estimates quoted in the tables are based on 95% confidence intervals derived from the residual errors in the monoexponential fits. Finally, the mean T_2 data across subjects, summarized in the last rows of Tables 1 and 2, are plotted in Figure 3, showing the average estimated GM and WM T_2 values, respectively, from 8-, 11-, and 22-msec refocusing interval acquisitions.

To investigate the effects of intersubject variability, tissue type, and refocusing rate, a three-factor ANOVA was performed. At $\alpha = 0.05$, the intersubject variability in estimated T_2 was not significant ($P = 0.97$). In contrast, there was a very strong effect of the tissue type on the T_2 estimate ($P < 10^{-5}$). The effect of the refocusing interval was also statistically significant ($P < 10^{-3}$), with the post hoc Tukey's analysis revealing a significantly different T_2 estimate from 22-msec acquisition as opposed to those from either 11- or 8-msec acquisitions. Specifically, the estimated T_2 decreased by an average of 3.3 ± 1.5 msec in GM and 3.0 ± 1.5 msec in WM between the 8- and 22-msec acquisitions. In both tissues, the T_2 dropped by 2.1 ± 1.4 msec between the 11- and 22-msec acquisitions.

Within-subject two-factor ANOVA, considering the effects of tissue type and refocusing rate, detected no statistically significant effect of the refocusing interval in any subject ($P > 0.34$). In 14 of 23 subjects, the effect of tissue type was statistically significant at $\alpha = 0.05$ (P

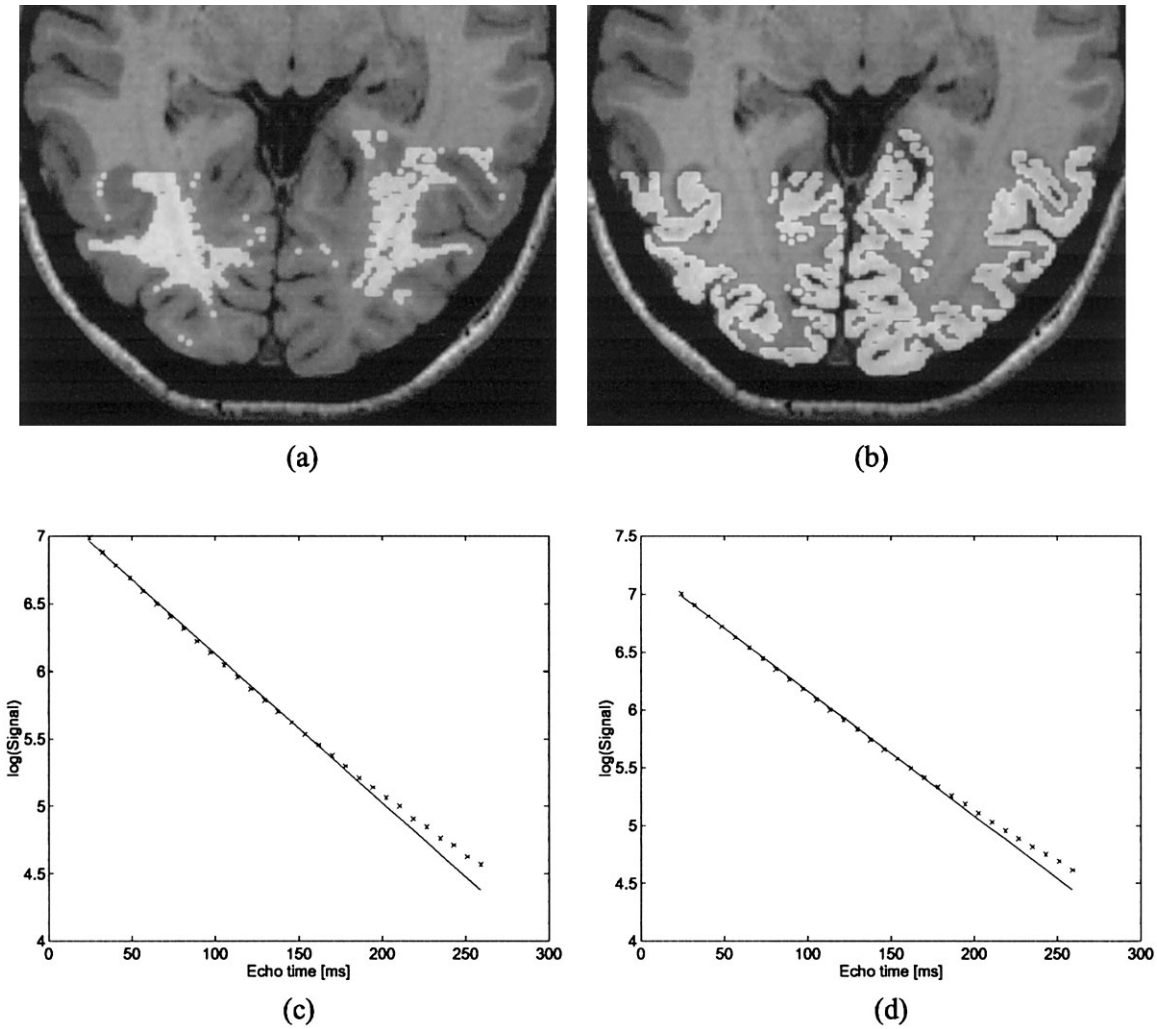

Figure 2. The WM (**a**) and GM (**b**) ROIs in the occipital lobe of a subject obtained by Bayesian classification followed by thresholding of the average estimated a posteriori probabilities at the 95% level. The logarithm of averaged ROI signal intensities at each echo time (shown as "x") and the logarithm of the corresponding nonlinear fits (shown as solid line) for the 8-msec refocusing interval acquisition for WM (**c**) and GM (**d**), respectively. Note the leveling off in the last few echoes due to Rician distributed noise.

< 0.024), with the GM T_2 being longer than that of WM for all subjects at all refocusing intervals.

DISCUSSION

The first finding of this study is the preservation of the common gray-white matter T_2 contrast in the occipital lobe of healthy adults. The results show a consistently longer T_2 in GM than in WM. While the estimated T_2 values certainly lie in the expected range for the respective tissues observed in numerous other studies (2,5,29–31), a different choice of ROI and/or averaging among a variety of areas, combined with the known heterogeneity of T_2 values hinders direct comparisons. The same contrast was also reported for an occipital lobe ROI at 3 T by Wansapura et al (4). However, at 1.5 T and with $1 \times 1.3 \times 2$ mm^3 resolution, Zhou et al observed an inversion of T_2 contrast between GM and WM (17). Bartha et al also reported shorter GM than WM T_2 values in the occipital lobe at both 4 T and 7 T (18).

It is important to consider the methodologic differences between these two studies (17,18) and the present work. Both studies had significantly different echo sampling than that used here: six echoes, 25 msec apart in the former (17); and four echoes for the short refocusing interval (6–7 msec) or three echoes for the long refocusing interval (10–26 msec) in the latter (18). The issues arising from few echoes in combination with monoexponential analysis have been well documented (32). Most notably, spurious statistically significant differences of 5%–15% were reported in estimated T_2 values depending on the number of echoes, echo spacing, and the timing of the first echo (32). On the other hand, a 32-echo 10-msec interecho interval CPMG sequence constitutes the de facto standard for in vivo T_2 relaxometry (5,26,32). Regarding the difference in the extent of the sampling, we have reanalyzed our data with sam-

Table 1
The Occipital WM T_2 Estimates From CPMG Acquisitions With Varied Refocusing Intervals

WM ROI (cc)	T^{8}_{2WM} (msec)	T^{11}_{2WM} (msec)	T^{22}_{2WM} (msec)
4.2	89 ± 1	87 ± 2	85 ± 3
5.4	85 ± 1	84 ± 2	83 ± 2
4.0	88 ± 2	87 ± 2	86 ± 3
7.4	80 ± 1	78 ± 1	80 ± 2
4.9	91 ± 2	90 ± 2	87 ± 4
5.4	90 ± 1	88 ± 1	85 ± 3
4.4	91 ± 2	89 ± 3	86 ± 4
7.4	87 ± 2	85 ± 2	84 ± 3
7.2	89 ± 2	87 ± 2	86 ± 3
4.2	82 ± 2	83 ± 2	81 ± 2
7.0	97 ± 2	96 ± 3	92 ± 4
3.6	93 ± 3	94 ± 3	91 ± 5
4.2	86 ± 1	83 ± 2	81 ± 2
6.1	85 ± 1	84 ± 1	82 ± 2
3.8	83 ± 1	83 ± 1	81 ± 2
2.4	83 ± 2	83 ± 2	80 ± 2
6.4	81 ± 1	81 ± 1	80 ± 2
1.5	86 ± 2	86 ± 2	84 ± 3
4.9	92 ± 2	91 ± 2	88 ± 3
3.5	91 ± 2	89 ± 2	86 ± 3
5.0	83 ± 1	82 ± 2	83 ± 2
4.4	92 ± 2	91 ± 2	87 ± 4
3.4	83 ± 2	84 ± 2	82 ± 2
4.8 ± 1.6	87 ± 4	86 ± 4	84 ± 3

pling windows aligned to those of Zhou et al (17) (thus truncating the data at 152 msec for the 8-msec refocusing data set, and at 154 msec for the 11- and 22-msec refocusing interval data sets). Notably, while the absolute values of all T_2 estimates decreased, all the conclusions still held: i.e., the usual T_2 tissue contrast was preserved for all subjects, at all refocusing intervals; there was a small but statistically significant effect of the refocusing interval, whereby the estimated T_2 decreased by an average 3 ± 1 msec in GM and 3 ± 2 msec in WM between 8- and 22-msec acquisitions.

Table 2
The Occipital GM T_2 Estimates From CPMG Acquisitions With Varied Refocusing Intervals

GM ROI (cc)	T^{8}_{2GM} (msec)	T^{11}_{2GM} (msec)	T^{22}_{2GM} (msec)
8.2	94 ± 2	92 ± 2	89 ± 4
7.8	89 ± 2	88 ± 2	87 ± 3
6.4	91 ± 2	89 ± 2	89 ± 4
6.7	87 ± 2	85 ± 2	87 ± 3
6.4	94 ± 2	92 ± 2	89 ± 3
7.8	100 ± 2	99 ± 3	95 ± 4
4.7	94 ± 2	93 ± 3	89 ± 4
8.0	91 ± 2	91 ± 2	89 ± 3
5.4	89 ± 2	88 ± 2	87 ± 3
2.9	87 ± 2	88 ± 2	85 ± 3
3.6	102 ± 3	100 ± 3	97 ± 4
6.6	94 ± 2	95 ± 3	92 ± 4
5.1	95 ± 2	94 ± 3	91 ± 3
8.3	94 ± 2	92 ± 2	90 ± 3
8.7	95 ± 2	93 ± 3	92 ± 4
4.0	91 ± 2	90 ± 2	87 ± 3
6.7	86 ± 2	87 ± 2	86 ± 2
3.2	87 ± 2	88 ± 2	85 ± 3
6.3	98 ± 2	96 ± 3	93 ± 4
7.8	92 ± 1	91 ± 2	88 ± 3
6.0	89 ± 2	87 ± 2	87 ± 3
5.8	95 ± 2	92 ± 2	90 ± 4
4.4	94 ± 3	93 ± 3	90 ± 5
6.1 ± 1.7	93 ± 4	91 ± 4	89 ± 3

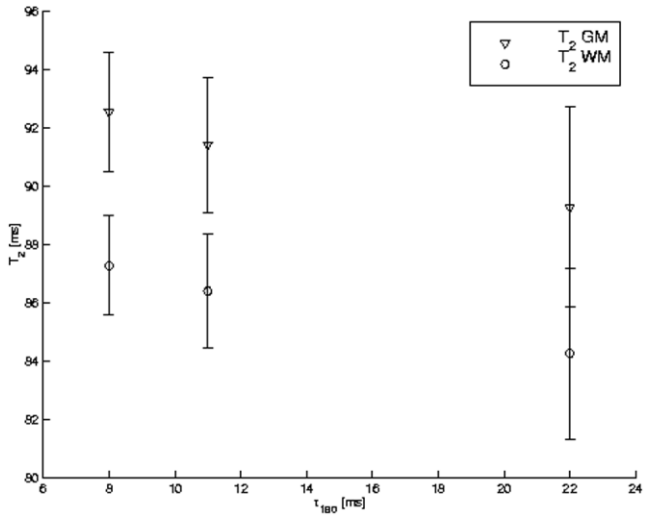

Figure 3. Average occipital GM and WM T_2 estimates from CPMG acquisitions with 8, 11 and 22 msec refocusing intervals. The error bars represent the SD of T_2 estimates across subjects.

We also noted that the subject age distribution in the study by Zhou et al (17) (32 ± 8 years) was different than the one in our investigation (29 ± 5 years), whereas the actual age ranges were quite similar (22 to 44 years in the former and 24 to 42 years in the latter). Although a very slow ferritin accumulation for either age range is expected in the occipital cortex based on the literature (11), we explored the effect of age on our T_2 estimates (both in terms of tissue T_2 contrast and the T_2 dependency on the refocusing interval) post hoc by looking at differences between the groups composed of the four youngest (24 ± 0 years) and the four oldest (38 ± 4 years) subjects in this study. We found a preserved, statistically significant ($P < 10^{-5}$) ordering of tissue T_2s (i.e., $T_{2GM} > T_{2WM}$), a trend of decreasing T_2 with increasing refocusing interval ($P > 0.4$), and no statistically significant effect of age ($P > 0.7$).

The difference in the ROI definition may also account for the differences in the findings. Specifically, the volumes of interest (for both GM and WM) in the study by Zhou et al (17) were much smaller than the ones used here. The authors employed two occipital ROIs of one to four voxels each, i.e., a volume of 0.0052–0.021 cc per tissue in each of the eight volunteers, with GM ROIs apparently located in the area of the primary visual cortex. The ROIs considered in this study, on the other hand, have an average (across the 23 subjects) volume of 4.8 ± 1.6 cc and 6.1 ± 1.7 cc in WM and GM, respectively (cf. Tables 1 and 2) and are composed of voxels originating across the occipital lobe section enclosed in the axial CPMG slice. We thus expect our GM T_2 values to reflect an average across the occipital cor-

tex and note that the variability in the occipital cortex cytoarchitecture, particularly the high density of granular cells and high degree of myelination of the primary visual cortex, may underlie the different T_2 GM vs. T_2 WM ordering.

Finally, while the T_2 data in the study by Zhou et al (17) was of higher resolution ($1 \times 1.3 \times 2$ mm^3) than that obtained with our CPMG acquisition ($1 \times 1 \times 5$ mm^3), it is important to note that the careful analysis was undertaken to ensure minimal partial volume errors in our ROIs. The segmentation was thus based on Bayesian classification of a $1 \times 1 \times 1$ mm^3 three-dimensional T_1-weighted acquisition. A very careful selection of the training data—namely, the selection of voxels within a very limited occipital VOI with separate training sets for each subject—is expected to provide very good Bayesian segmentation (27). Indeed, a validation of the parametric Bayesian classification showed robust performance with respect to noise, RF inhomogeneities, and slice thickness (33). Moreover, minimal intensity nonuniformities arise in our very limited occipital VOI. We thus expect excellent performance of the Bayesian segmentation and, based on visual inspection, very good spatial coincidence between the high resolution three-dimensional *T*1-weighted scan and the two-dimensional CPMG data, thereby ensuring a very low CSF contamination of our ROIs (with average normalized a posteriori probability of CSF in the GM ROI of $0.6 \pm 0.4\%$) and a correspondingly high sensitivity to the intrinsic contrast between GM and WM (that might otherwise be obscured by partial voluming between GM and CSF). Overall, given our substantial subject pool, large number of echoes, extensive ROIs, and very low partial voluming, we feel confident of the presented occipital T_2 estimates. We also note that our experimental results agree well with the preliminary theoretical predictions of tissue T_2 (of 92 msec for T_{2GM} and 87 msec for T_{2WM}) presented by Zhou et al (17) and based on the water content, myelin water fraction, and blood volume of GM and WM, respectively.

The second major finding of the present work is the statistically significant effect, after controlling for intersubject variability, of the CPMG refocusing interval on the occipital tissue T_2 estimates at 1.5 T. The small decrease, of $3 \pm 2\%$, in the T_2 values of either tissue can be accounted for by the effect of blood. (It is worth noting that the very small blood content of either tissue, as well as proximity of T_2 of blood to those of tissue at 1.5 T, precludes biexponential modeling of in vivo data: the monoexponential decay model is thus applied to ROIs composed of both tissue and blood.) Specifically, the confinement of paramagnetic dHb to red blood cells gives rise to two vascular compartments with distinct magnetic properties: the intraerythrocytic and the plasmatic. The exchange of water spins between these two environments—with exchange time of 6 to 8 msec (34,35)—causes a Larmor frequency shift which, in turn, results in enhancement of the blood R_2 (36). Following Luz and Meiboom's model of chemical exchange between multiple sites at different frequencies (37) to describe this dependency, the R_2 of blood (R_{2b}) is given by (22):

$$R_{2b} = R_{2_0} + \mathrm{Hct}(1 - \mathrm{Hct})\,(\Delta\omega)^2\tau_{ex}\left(1 - \frac{2\tau_{ex}}{\tau_{180}}\tanh\frac{\tau_{180}}{2\tau_{ex}}\right), \quad (1)$$

where R_{2_0} is the intrinsic R_2 of blood; Hct is the hematocrit; τ_{ex} is the average exchange time; and τ_{180} is the refocusing interval. The frequency shift resulting from the different susceptibilities of the two compartments, $\Delta\omega$, depends on the level of blood oxygenation (22):

$$\Delta\omega = \eta\left(1 - \frac{Y}{100}\right)\omega_0, \quad (2)$$

where ω_0 is the Larmor frequency; η is a dimensionless constant determined by the shape and spacing of dHb-containing erythrocytes, as well as the susceptibility of dHb; and Y is the blood percent oxygenation. Parameterizing these equations with physiologic values from the literature (1), the T_2 of venous blood (having oxygen saturation of ~60% [1]) decreases by ~45% between the 8- and 22-msec refocusing interval acquisitions, in accordance with the published values from in vitro experiments (22). Thus, even with the small blood content of the tissue (~6% for GM and ~4% for WM [1]), a change in the observed T_2 is expected. Assuming a slow exchange across the capillary wall, the normalized signal from a voxel composed of either WM or GM and blood is:

$$\frac{S}{S_0} = x_t e^{-R_{2t}TE} + x_b e^{-R_{2b}TE}, \quad (3)$$

where x_t and x_b are tissue and blood water volume fractions, respectively. Furthermore, the blood component is composed of arteriolar, capillary, and venous contributions, with respective volume fractions and oxygen saturation levels set to literature values (1). Fitting the signal values predicted by this biexponential equation to the monoexponential decay model, the T_2 estimate decreases by 3 msec in GM and 2 msec in WM between the 8- and 22-msec refocusing interval acquisitions, in excellent agreement with our observed in vivo drop of 3.3 ± 1.5 msec in GM and 3.0 ± 1.5 msec in WM. The presence of paramagnetic dHb attenuates the extravascular signal as well, due to diffusion of tissue spins in the local magnetic field gradients surrounding the partially deoxygenated blood vessels. However, the extravascular effect of dHb is minimized (1) by the employment of the train of refocusing pulses in the CPMG acquisitions used here.

On the other hand, there are potential extravascular sources of tissue T_2 dependence on the refocusing interval. Notably, the heterogeneously distributed ferritin, with its antiferromagnetic core (38), is expected to induce local magnetic field perturbations, thereby shortening the T_2. Indeed, pronounced T_2 decreases have been observed in the extrapyramidal system in a number of brain iron studies (8–10). However, the importance of the ferritin's relaxivity effect relative to other in vivo transverse relaxation mechanisms remains disputed (14,15). Finally, the occipital cortex has a low nonheme iron content (an average 4.55 ± 0.67 mg of

iron per 100 g of fresh weight [11]) compared to that of the extrapyramidal system (with a mean of 15.36 ± 4.86 mg of iron/100 g fresh weight [11]).

In spite of an expected increase in ferritin's relaxivity at higher fields, it is questionable whether ferritin accumulation alone can account for the dramatic (30%–40%) refocusing interval dependent variation of occipital tissue T_2 estimates, observed by Bartha et al (18) at 4 T and 7 T, between the short ($\tau_{180} < 10$ msec) and long ($\tau_{180} > 10$ msec) refocusing interval acquisitions. In particular, they reported strong refocusing rate dependence of occipital WM T_2 despite the extremely low concentration of ferritin in the occipital WM (39,40), as well as similar WM and GM T_2 drops despite a large difference in the tissues' ferritin contents. Both of these propound a source of magnetic inhomogeneities other than ferritin. Irrespective of the origin of the observed relaxation enhancement, however, the degree of the T_2 shortening and the range of refocusing intervals over which it occurs depend on the nature of the underlying transverse relaxation enhancement mechanism as well as the strength of the external magnetic field. Hence, due to the lack of definitive knowledge about the underlying mechanism(s), an extrapolation of the 4 T and 7 T data to 1.5 T is not available. While the limited T_2 shortening with increasing refocusing interval observed here at 1.5 T most likely arises from the changes in the T_2 of the partly deoxygenated blood in the ROIs, we cannot rule out more pronounced occipital tissue T_2 shortening at higher fields, possibly due to a combination of relaxation mechanisms. Nevertheless, the small observed magnitude of the T_2 shortening at 1.5 T for the refocusing intervals of interest provides support for our CBV methodology (24). The isolation of the blood signal in that method, allowing for quantification of CBV changes accompanying functional activation, is achieved through variation of the refocusing interval, at constant echo time, in neighboring measurements, thus relying on the uniqueness of T_{2blood} dependency on the refocusing interval in the range of refocusing intervals explored here.

In conclusion, we have observed the common gray-white matter T_2 contrast (i.e., $T_{2GM} > T_{2WM}$) in the occipital lobe and a small, but a statistically significant ($P < 10^{-3}$) decrease of tissue transverse relaxation time with increasing CPMG refocusing interval (3.3 ± 1.5 msec drop in T_2 of GM and 3.0 ± 1.5 msec drop in T_2 of WM for refocusing interval elongation from 8 to 22 msec). The estimated T_2 values lie in the expected range based on the earlier T_2 relaxometry studies and are in close agreement with theoretical GM and WM tissue T_2 calculated from estimates of the water content, myelin water fraction, and blood volume of each tissue (17). The observed shortening of the estimated T_2 can be accounted for by the known effect of refocusing interval on the T_2 of partly deoxygenated blood. The results also lend support to the hypothesis of a refocusing rate independent T_2 of extravascular brain tissue at 1.5 T.

REFERENCES

1. van Zijl PCM, Eleef SM, Ulatowski JA, et al. Quantitative assessment of blood flow, blood volume and blood oxygenation effects in functional magnetic resonance imaging. Nat Med 1998;4:159–167.
2. Gersonde K, Tolxdorff T, Felserg L. Identification and characterization of tissues by T_2-selective whole-body proton NMR imaging. Magn Reson Med 1985;2:390–401.
3. Breger RK, Wehrli FW, Charles HC, MacFall JR, Haughton VM. Reproducibility of relaxation and spin-density parameters in phantoms and the human brain measured by MR imaging at 1.5T. Magn Reson Med 1986;3:649–662.
4. Wansapura JP, Holland SK, Dunn RS, Ball WS. NMR relaxation times in the human brain at 3.0 Tesla. J Magn Reson Imaging 1999;9:531–538.
5. Whittall KP, MacKay AL, Graeb DA, Nugent RA, Li DKB, Paty DW. In vivo measurement of T_2 distributions and water contents in normal human brain. Magn Reson Med 1997;37:34–43.
6. Georgiades CS, Itoh R, Golay X, van Zijl PCM, Melhem ER. MR imaging of the human brain at 1.5T: regional variations in transverse relaxation rates in the cerebral cortex. AJNR Am J Neuroradiol 2001;22:1732–1737.
7. Ferrie JC, Barantin L, Saliba E, et al. MR assessment of the brain maturation during the perinatal period: quantitative T_2 MR study in premature newborns. Magn Reson Imaging 1999;17:1275–1288.
8. Ye FQ, Wayne Martin WR, Allen PS. Estimation of the iron concentration in excised gray matter by means of proton relaxation measurements. Magn Reson Med 1996;35:285–289.
9. Vymazal J, Brooks RA, Baumgarner C, et al. The relation between brain iron and NMR relaxation times: an in vitro study. Magn Reson Med 1996;35:56–61.
10. Gelman N, Gorell JM, Barker PB, et al. MR imaging of human brain at 3.0T: preliminary report on transverse relaxation rates and relation to estimated iron content. Radiology 1999;210:759–767.
11. Hallgren B, Sourander P. The effect of age on the non-haemin iron in the human brain. J Neurochem 1958;3:41–51.
12. Hirai T, Korogi Y, Sakamoto Y, Hamatake S, Ikushima I, Takahashi M. T_2 shortening in the motor cortex: effect of aging and cerebrovascular diseases. Radiology 1996;199:799–803.
13. Yoshiura T, Higano S, Rubio A, et al. Heschl and superior temporal gyri: low signal intensity of the cortex on T_2-weighted MR images of the normal brain. Radiology 2000;214:217–221.
14. Chen JC, Hardy PA, Clauberg M, et al. T_2 values in the human brain: comparison with quantitative assays of iron and ferritin. Radiology 1989;173:521–526.
15. Chen JC, Hardy PA, Kucharczyk W, et al. MR of human postmortem brain tissue: correlative study between T_2 and assays of iron and ferritin in Parkinson and Huntington disease. Am J Neuroradiol Res 1993;14:275–281.
16. Brooks RA, Luthert P, Gadian D, Marsden CD. Does signal-attenuation on high-field T_2-weighted MRI of the brain reflect regional cerebral iron deposition? Observations on the relationship between regional cerebral water proton T_2 values and iron levels. J Neurol Neurosurg Psychiatry 1989;52:108–111.
17. Zhou J, Golay X, van Zijl PCM, et al. Inverse T_2 contrast at 1.5 Tesla between gray matter and white matter in the occipital lobe of normal adult human brain. Magn Reson Med 2001;46:401–406.
18. Bartha R, Michaeli S, Merkle H, et al. In vivo H_2O T_2 measurement in the human occipital lobe at 4T and 7T by Carr-Purcell MRI: detection of microscopic susceptibility contrast. Magn Reson Med 2002;47:742–750.
19. Jensen JH, Chandra R, Yu H. Quantitative model for the interecho time dependence of the CPMG relaxation rate in iron-rich gray matter. Magn Reson Med 2001;46:159–165.
20. Hardy PA, Henkelman RM. Transverse relaxation rate enhancement caused by magnetic particulates. Magn Reson Imaging 1989; 7:265–275.
21. Thulborn K, Waterton JC, Matthews P, Radda G. Oxygenation dependence of the transverse relaxation time of water protons in the whole blood at high field. Biochim Biophys Acta 1982;714:265–270.
22. Wright GA, Nishamura DG, Macovski A. Flow-independent magnetic resonance projection angiography. Magn Reson Med 1991;16: 126–140.
23. Golay X, Silvennoinen MJ, Zhou J, et al. Measurement of tissue oxygen extraction ratios from venous blood T_2: increased precision and validation of principle. Magn Reson Med 2001;46:282–291.
24. Stefanovic B, Pike GB. Quantitative dynamic measurement of cerebral blood volume changes via fMRI. In: Proceedings of the 10th Annual Meeting of ISMRM, Honolulu, 2002. p 119.

25. Fenrich FRE, Beaulieu C, Allen PS. Relaxation times and microstructures. NMR Biomed 2001;14:133–139.
26. Poon CS, Henkelman RM. Practical T_2 quantitation for clinical applications. J Magn Reson Imaging 1992;2:541–553.
27. Bezdek JC, Hall LO, Clarke LP. Review of MR image segmentation techniques using pattern recognition. Med Phys 1993;20:1033–1048.
28. Duda RO, Hart PE. Pattern recognition and scene analysis. Wiley: New York; 1973.
29. Breger RK, Rimm AA, Fischer ME, Papke RA, Haughton VM. T_1 and T_2 measurements on a 1.5-T commercial MR imager. Radiology 1989;171:273–276.
30. Bottomley PA, Foster TH, Argersinger RE, Pfeifer LM. A review of normal tissue hydrogen NMR relaxation times and relaxation mechanisms from 1–100 MHz: dependence on tissue type, NMR frequency, temperature, species, excision, and age. Med Phys 1984;11:425–448.
31. Larsson EM, Englund E, Gyorffy-Wagner Z, Brun A, Cronqvist S, Persson B. Regional differences in the proton magnetic resonance relaxation times T_1 and T_2 within the normal human brain. Acta Radiol Diagnosis 1986;27:231–234.
32. Whittall KP, MacKay AL, Li DKB. Are mono-exponential fits to a few echoes sufficient to determine T_2 relaxation for in vivo human brain? Magn Reson Med 1999;41:1255–1257.
33. Kollokian V. Performance analysis of automatic techniques for tissue classification in MRI of the human brain. Thesis, Concordia University, Montreal, Canada, 1996.
34. Brooks RA, DiChiro G. Magnetic resonance imaging of stationary blood: a review. Med Phys 1987;14:903–913.
35. Conlon T, Outhred R. Water diffusion permeability of erythrocytes using an NMR technique. Biochim Biophys Acta 1972;288:354–361.
36. Bryant RG, Marill K, Blackmore C, Francis C. Magnetic relaxation in blood and blood clots. Magn Reson Med 1990;13:133–144.
37. Luz Z, Meiboom S. Nuclear magnetic resonance study of the protolysis of trimethylammonium ion in aqueous solution—order of the reaction with respect to the solvent. J Chem Physics 1963;39:366–370.
38. Brooks RA, Vymazal J, Goldfarb RB, Bulte JWM, Aisen P. Relaxometry and magnetometry of ferritin. Magn Reson Med 1998;40:227–235.
39. Hoeck A, Demmel U, Schicha H, Kasperek K, Feinendegen L. Trace element concentration in human brain. Brain 1975;98:49–64.
40. Drayer B, Burger P, Darwin R, Riederer S, Herfkens R, Johnson G. MRI of brain iron. AJR Am J Roentgenol 1986;147:103–110.